

Hydrodynamic stability of a thin volatile liquid film

S. Rossomme, B. Scheid and P. Colinet

Université Libre de Bruxelles, Service de Chimie Physique E.P.,
 Faculté des Sciences Appliquées, CP 165/62, Avenue F.D. Roosevelt, 50 - 1050 Bruxelles
 email: srossomm@ulb.ac.be, bscheid@ulb.ac.be, pcolinet@ulb.ac.be

Abstract—This paper deals with the nonlinear evolution of a thin liquid film in contact with a hot rigid plate. The liquid phase is separated from its own vapour by a deformable interface. Various mechanisms affect the stability of the film and govern its shape. Among them, we focus on the surface tension and its variation with temperature, the evaporation and the resulting vapour recoil pressure resulting from momentum conservation at the interface, the disjoining pressure resulting from molecular interactions with the substrate, the temperature discontinuity between vapour and liquid at the interface and the variation of the saturation temperature due to the disjoining pressure and the interfacial curvature. We show how the contact angle and the heat flux vary with some of these effects.

Keywords—Thin films, Disjoining pressure, Surface tension, Thermocapillarity, Chemical and thermal non-equilibrium effects, Stability.

I. INTRODUCTION

THIN and ultra-thin liquid films are a subject of intensive research nowadays, as they intervene in many scientific areas such as in biophysics, micro-fluidics and nanotechnologies. In particular, thin films are of primary importance in heat transfer technologies based on evaporation or boiling. As demonstrated by Stephan and Busse [1], most of the heat (and mass) flux indeed occurs in the vicinity of contact lines, i.e. transition regions between a liquid volume and a thin film adsorbed on the heater.

Burelbach et al. [2] developed a model describing the temporal evolution of the film thickness and analysed the film stability. Their model accounts for the following effects: mass loss (gain), vapour recoil, thermocapillarity, viscous forces, surface tension and molecular forces due to Van der Waals interactions with the substrate. The purpose of this paper is to generalize Burelbach's model by including various effects. First, following Stephan's work, we consider the saturation temperature at the interface to depend on the disjoining pressure and the curvature of the interface. Rigorously, the recoil pressure and the viscous stress could also influence the saturation temperature but, for the conditions studied on this paper, their role is negligible. Note that, when the molecular interactions are opposed to evaporation, a flat non-evaporating film of microscopic thickness is possible. One of the purposes of the present paper is to study its stability. Secondly, using the laws of non-equilibrium thermodynamics for interfaces, we relax the assumption that liquid and vapour temperatures were equal. This jump of temperature was studied theoretically (with a general thermodynamic modelling) by Bedeaux [3] and experimentally, during steady-state liquid evaporation, by Fang and Ward [4]. Thirdly, our model will also take into account the thermal conductivity of the solid wall [5].

The structure of the paper is the following. In Section II, the set of governing equations is established, and a lubrication-type model is derived. In Section III, we perform a linear stability analysis in a simplified case (no influence of Van der Waals repulsion, negligible thermal resistance of the wall and conductivity of vapour phase). Section IV presents the numerical results for the complete model. Finally, conclusions are outlined in Section V.

II. MODEL

We consider a thin viscous liquid layer bounded above by its own vapour and below by a uniformly heated rigid plate. The unknown position of the vapour-liquid interface (z) is described by a function of the coordinates x , y and time t : $z = \xi(x, y, t)$.

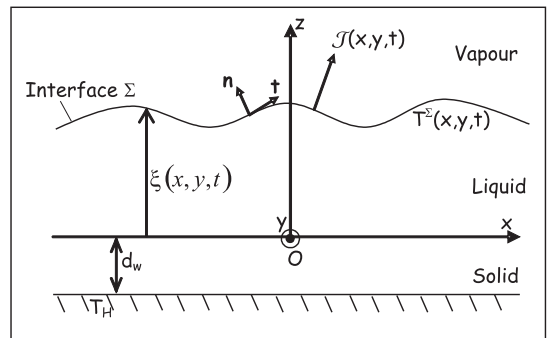


Fig. 1. The studied system is composed of a rigid substrate on which lies a volatile liquid film. The latter is in contact with its own vapour at the interface $z = \xi(x, y, t)$.

Fig. 1 shows the configuration of the problem and the Cartesian coordinate system (x, y, z) with the origin at the wall. $\mathcal{J}(x, y, t)$ is the interfacial mass flux, $T^{(\Sigma)}$ is the temperature of the interface, and T_H is the constant temperature of the heated plate at $z = -d_w$ with d_w the thickness of the solid. The normal unit vector, oriented towards the vapour, is $\mathbf{n} = (-\nabla\xi, 1)(1 + |\nabla\xi|^2)^{-1/2}$ where $\nabla = (\partial_x, \partial_y)$ and the tangent unit vectors are $\mathbf{t}_1 = (1, 0, \partial_x\xi)(1 + (\partial_x\xi)^2)^{-1/2}$, $\mathbf{t}_2 = (0, 1, \partial_y\xi)(1 + (\partial_y\xi)^2)^{-1/2}$. Some quantities may be discontinuous across the liquid-vapour interface. If q is one of these quantities, we will note its value in the vapour and liquid phase respectively by q_v and q_l , with $\{q\}_- = q_v - q_l$.

The liquid layer is laterally unbounded and thin enough so that gravity effects are negligible. We assume that the liquid is Newtonian, incompressible and that its properties (except the surface tension) are constant. We also consider that the density (ρ) and the dynamic viscosity (η) are both much greater in the liquid than in the vapour [2]. Formally,

we assume:

$$\frac{\rho_v}{\rho_l} \rightarrow 0 \quad \frac{\eta_v}{\eta_l} \rightarrow 0$$

A. Governing equations

Flow of the liquid is described by the equation of continuity, the momentum balance (Navier-Stokes) and the energy balance. Under the hypotheses above, they read, respectively,

$$\nabla \cdot \mathbf{v}_l = 0 \quad (1)$$

$$\rho_l (\partial_t \mathbf{v}_l + \mathbf{v}_l \cdot \nabla \mathbf{v}_l) = -\nabla p_l + \eta_l \Delta \mathbf{v}_l \quad (2)$$

$$\partial_t T_l + \mathbf{v}_l \cdot \nabla T_l = \kappa_l \Delta T_l \quad (3)$$

where ρ_l is the liquid density, η_l is the liquid dynamic viscosity and κ_l is the liquid thermal diffusivity. p_l denotes the liquid pressure, \mathbf{v}_l is the liquid velocity vector with components u, v, w in the x -, y - and z -directions, and T_l is the liquid temperature. Eqs(1-3) are valid for $0 \leq z \leq \xi$. The solid is taken into account [5] by coupling the equation (3) with the thermal conduction equation in the solid for $-d_w \leq z \leq 0$, written in the quasi-steady approximation

$$\Delta T_s = 0$$

where T_s is the solid temperature.

B. Boundary conditions

Eqs(1-3) should be completed by suitable boundary conditions: [5, 7]

B.1 At the walls ($z = 0$ and $z = -d_w$)

At the heated solid boundary ($z = 0$), we assume no-slip condition:

$$\mathbf{v} = 0$$

For the temperature, there are 3 boundary conditions. Firstly, two at $z = 0$ to ensure the conditions of continuity of both the solid and liquid temperatures and solid and liquid heat fluxes

$$T_s = T_l \quad -\lambda_s \partial_z T_s = -\lambda_l \partial_z T_l$$

and secondly, one at $z = -d_w$ to impose a uniform temperature at the other side of the solid $T_s = T_H$.

B.2 At the free surface ($z = \xi(x, y, t)$)

At the liquid-vapour interface, the boundary conditions are conservations of mass, momentum and energy completed by the kinematic condition [7]. The latter reads

$$\mathbf{v}_\Sigma \cdot \mathbf{n} = \frac{\partial_t \xi}{\sqrt{1 + (\nabla \xi)^2}} \quad (4)$$

where \mathbf{v}_Σ is the velocity of the interface.

The jump mass balance is

$$\mathcal{J} = \rho_v (\mathbf{v}_v \cdot \mathbf{n} - \mathbf{v}_\Sigma \cdot \mathbf{n}) = \rho_l (\mathbf{v}_l \cdot \mathbf{n} - \mathbf{v}_\Sigma \cdot \mathbf{n}) \quad (5)$$

where \mathbf{v}_v is the vapour velocity and ρ_v is the vapour density.

As the fluid is incompressible and Newtonian, we can write the stress tensor: $\underline{T} = -p\underline{I} + 2\eta\underline{d}$ where \underline{I} is the identity tensor, p the pressure, η the dynamic viscosity and \underline{d} the rate of deformation tensor. If we suppose that the surface tension decreases linearly with the temperature, we have the equation of state: $\gamma = \gamma_r - \gamma_r^s (T^{(\Sigma)} - T_{sat})$ where γ_r is the surface tension at the reference temperature T_{sat} and $T^{(\Sigma)} = T_l|_{z=\xi}$.

With these properties, the momentum jump is

$$\mathcal{J}\{\mathbf{v}\}_- - \{\underline{T} \cdot \mathbf{n}\}_- - p_d \cdot \mathbf{n} = \nabla_s \gamma - \gamma (\nabla_s \cdot \mathbf{n}) \mathbf{n} \quad (6)$$

where $\nabla_s = (\underline{I} - \mathbf{n}\mathbf{n}) \cdot \nabla$ is the surface gradient operator and p_d is the disjoining pressure. This concept was set out by Derjaguin [8] to quantify the interactions between a thin film and its interfaces (solid and/or gas). In this work, we shall use the Lennard-Jones potential. Consequently, the disjoining pressure reads [9]

$$p_d = \frac{A}{\xi^3} - \frac{R}{\xi^9}$$

where the first term is the attraction and the second is the repulsion. Here, we will consider the case $A > 0$ and $R < 0$ which corresponds to a stabilising Van der Waals force. The projection of Eq.(6) on the normal gives the expression of the normal stress boundary condition

$$-p_v + p_d + p_l - \mathbf{n} \cdot \underline{T}_l \cdot \mathbf{n} = p_\sigma + \frac{\mathcal{J}^2}{\rho_v} \quad (7)$$

where $p_\sigma = -2\gamma K$ and the mean film surface curvature K is defined by [7]

$$K = -\frac{\nabla_s \cdot \mathbf{n}}{2} = \frac{\partial_{xx}^2 \xi (1 + (\partial_y \xi)^2) + \partial_{yy}^2 \xi (1 + (\partial_x \xi)^2) - 2\partial_x \xi \partial_y \xi \partial_{xy}^2 \xi}{2[1 + (\partial_x \xi)^2 + (\partial_y \xi)^2]^{3/2}}$$

The projection of Eq.(6) on the tangents ($i = 1, 2$) gives

$$\mathbf{n} \cdot \underline{T}_l \cdot \mathbf{t}_i = \nabla_s \gamma \cdot \mathbf{t}_i = \frac{\sigma_i}{(1 + \xi_i^2)^{1/2}} = \frac{\partial \sigma}{\partial T} \frac{\partial_i T + \partial_i \xi \partial_z T}{(1 + \xi_i^2)^{1/2}} \quad (8)$$

The jump energy balance is

$$\mathcal{J} \left\{ \mathcal{L} + \frac{1}{2} [(\mathbf{v}_v - \mathbf{v}_\Sigma) \cdot \mathbf{n}]^2 - \frac{1}{2} [(\mathbf{v}_l - \mathbf{v}_\Sigma) \cdot \mathbf{n}]^2 \right\} + \lambda_l \nabla T_l \cdot \mathbf{n} - \lambda_v \nabla T_v \cdot \mathbf{n} - \underline{\tau}_v (\mathbf{v}_v - \mathbf{v}_\Sigma) \cdot \mathbf{n} + \underline{\tau}_l (\mathbf{v}_l - \mathbf{v}_\Sigma) \cdot \mathbf{n} = 0$$

where λ_l and λ_v are the thermal conductivities of the liquid and of the vapour, \mathcal{L} is the vaporisation latent heat. If we neglect viscous and kinetic energy effects, the energy balance at the interface gives

$$\{J_q\}_- = -\mathcal{L}\mathcal{J} \quad (9)$$

where

$$J_{q,l} = -\nabla T_l \cdot \mathbf{n} \quad (10)$$

$$J_{q,v} = -\lambda \nabla T_v \cdot \mathbf{n} \quad (11)$$

The last two boundary conditions arise from the irreversible thermodynamics, in particular from the interfacial

entropy production (σ^s). If we suppose that the evaporation is slow, σ^s is [3]

$$\sigma^s = \left\{ [J_q + \mathcal{J}sT] \left[\frac{1}{T} - \frac{1}{T(\Sigma)} \right] \right\}_- - \frac{\{\mathcal{J}(\mu - \mu^s)\}_-}{T(\Sigma)} \quad (12)$$

where s is the entropy, μ and μ^s are the liquid and the interfacial chemical potential. According to the equation (12), the interfacial behaviour is governed by two generalized forces (the differences of temperature and of chemical potential). Developing Eq.(12) and using $\mathcal{L} = h_v - h_l$ and $h_v = \mu_v + T_v s_v$ and $h_l = \mu_l + T_l s_l$, we obtain

$$\sigma^s = -J_{q,v} \frac{1}{T_v T_l} \{T\}_- - \mathcal{J} \frac{1}{T_l} (s_v \{T\}_- + \{\mu\}_-) \quad (13)$$

We assume that T_v and T_l are close to a temperature of reference (T_r) and we develop at first order. Then, developing the second term (details will be published elsewhere) and assuming that $T_r = T_{sat}$, $T_l = T_r + \delta T_l$ and $T_v = T_r + \delta T_v$, we obtain the two interfacial constitutive relations. They give the two generalized fluxes in the non-equilibrium state, that read

$$\begin{cases} J_{q,v} = -L_{qq} \frac{1}{T_{sat}^2} \{T\}_- + L_{qw} \frac{\mathcal{L}}{T_{sat}^2} (T_l - T_{sat,loc}) \\ \mathcal{J} = -L_{wq} \frac{1}{T_{sat}^2} \{T\}_- + L_{ww} \frac{\mathcal{L}}{T_{sat}^2} (T_l - T_{sat,loc}) \end{cases} \quad (14)$$

where L_{qq} , L_{ww} , L_{qw} and L_{wq} are phenomenological coefficients. $L_{qw} = L_{wq}$ according to the Onsager-Casimir reciprocity relations [10]. With the second principle L_{qq} and L_{ww} must be positive and $L_{qq}L_{ww} \geq L_{qw}^2$. $T_{sat,loc}$ includes the modification of the saturation temperature at the interface because of some microscopic effects (disjoining pressure and curvature) that cannot be neglected [1]

$$T_{sat,loc} = T_{sat} \left(1 + \frac{p_d - p_\sigma}{\rho_l \mathcal{L}} \right) \quad (15)$$

C. Dimensionless equations and parameters

We choose ξ_0 , $\frac{\xi_0^2}{\nu_l}$, $\frac{\rho_l \nu_l^2}{\xi_0^2}$, $\frac{\lambda_l \Delta T}{\xi_0 \mathcal{L}}$ and $\frac{\lambda_l \Delta T}{\xi_0}$ to scale the length, time, velocity, pressure, mass flux and heat flux, with ξ_0 a characteristic thickness and $\Delta T = (T_H - T_{sat})$. The dimensionless temperature (noted T in the following) is defined by $\frac{T - T_{sat}}{\Delta T}$. With these definitions, the dimensionless equations are expressed as follows.

C.1 Liquid phase equations

$$\nabla \cdot \mathbf{v}_l = 0 \quad (16)$$

$$\partial_t \mathbf{v}_l + \mathbf{v}_l \cdot \nabla \mathbf{v}_l = -\nabla p_l + \Delta \mathbf{v}_l \quad (17)$$

$$\partial_t T_l + \mathbf{v}_l \cdot \nabla T_l = P^{-1} \Delta T_l \quad (18)$$

C.2 Boundary conditions

- At the liquid-substrate interface ($z = 0$):

$$u_l = v_l = w_l = 0 \quad (19)$$

$$T_s = T_l \quad (20)$$

$$-\lambda_s \partial_z T_s = -\lambda_l \partial_z T_l \quad (21)$$

- At the bottom of the substrate ($z = -\frac{d_w}{\xi_0}$):

$$T_s = 1 \quad (22)$$

- At the interface ($z = \xi(x, y, t)$):

Kinematic condition:

$$\mathbf{v}_\Sigma \cdot \mathbf{n} = \frac{\partial_t \xi}{\sqrt{1 + (\nabla \xi)^2}} \quad (23)$$

Conservation laws:

$$E\mathcal{J} = (\mathbf{v}_l - \mathbf{v}_\Sigma) \cdot \mathbf{n} = \frac{2}{3} D (\mathbf{v}_v - \mathbf{v}_\Sigma) \cdot \mathbf{n} \quad (24)$$

$$p_d + p_l - \mathbf{n} \cdot \underline{\underline{T}}_l \cdot \mathbf{n} = (3S - 2MP^{-1}T_l) \nabla_s \cdot \mathbf{n} + p_v + \frac{3}{2} E^2 D^{-1} \mathcal{J}^2 \quad (25)$$

$$\mathbf{n} \cdot \underline{\underline{T}}_l \cdot \mathbf{t}_i = -MP^{-1} \nabla T_l \cdot \mathbf{t}_i \quad (26)$$

$$\mathcal{J} = -\nabla T_l \cdot \mathbf{n} + \lambda \nabla T_v \cdot \mathbf{n} \quad (27)$$

Note that in Eq.(25), $p_v = p_s(T_{sat})$ is by definition constant, neglecting hydrodynamics stresses in the vapour. We can extract T_v and T_l from phenomenological laws (14), which results in the following dimensionless equations:

$$T_v = -H_r J_{q,v} + T_l (1 + H_c) - \phi H_c (p_d - p_\sigma) \quad (28)$$

$$T_l = H_j H_c J_{q,v} - H_j \mathcal{J} + \phi (p_d - p_\sigma) \quad (29)$$

The dimensionless parameters that appear in the above equations are defined in Table I.

TABLE I
DIMENSIONLESS PARAMETERS.

Ratio of the vapour to liquid densities: $D = \frac{3}{2} \frac{\rho_v}{\rho_l}$
Evaporation number: $E = \frac{\lambda_l \Delta T}{\nu_l \mathcal{L} \rho_l}$
Marangoni number: $M = \frac{\gamma_r^s \Delta T \xi_0}{2 \rho_l \nu_l \kappa_l}$
Prandtl number: $P = \frac{\nu_l}{\kappa_l}$
Surface tension: $S = \frac{\gamma_r \xi_0}{3 \rho_l \nu_l^2}$
Ratio of the vapour to liquid thermal conductivities: $\lambda = \frac{\lambda_v}{\lambda_l}$
Influence of the disjoining pressure and the curvature over the saturation temperature: $\phi = \frac{T_{sat} \nu_l^2}{\mathcal{L} \Delta T \xi_0^2}$
Influence of the thermal conductivity of the solid: $CS = \frac{d_w \lambda_l}{\xi_0 \lambda_s}$
Interfacial transfer parameters:
$H_r = \frac{\lambda_l T_{sat}^2}{L_{qq} \xi_0}$
$H_c = \frac{L_{qw} \mathcal{L}}{L_{qq}}$
$H_j = \frac{L_{qq} \lambda_l T_{sat}^2}{(L_{qw}^2 - L_{qq} L_{ww}) \xi_0 \mathcal{L}^2}$

D. Long-wave theory

Assuming that the space variations along x and y are much slower than those in the z -direction, we can apply the long-wave theory [2, 5]. We define a small parameter ε that is

the ratio between the mean film thickness and the characteristic wavelength of horizontal modulations: $\varepsilon = \frac{\xi_0}{\lambda} \ll 1$. We then rescale space and time variables as

$$\alpha = \varepsilon x \quad \beta = \varepsilon y \quad \omega = z \quad \iota = \varepsilon t$$

If we assume that $u, v, \mathcal{J}, T = \mathcal{O}(1)$, due to the equation of continuity $w = \mathcal{O}(\varepsilon)$. In order to be able to keep the influence of the pressure terms, we take $p, p_d, p_\sigma = \mathcal{O}(\varepsilon^{-1})$. All variables are expanded in powers of ε :

$$\begin{aligned} u &= u_0 + \varepsilon u_1 + \dots & v &= v_0 + \varepsilon v_1 + \dots \\ w &= \varepsilon(w_0 + \varepsilon w_1 + \dots) & T &= T_0 + \varepsilon T_1 + \dots \\ J_q &= J_{q,0} + \varepsilon J_{q,1} + \dots & \mathcal{J} &= \mathcal{J}_0 + \varepsilon \mathcal{J}_1 + \dots \\ p &= \varepsilon^{-1}(p_0 + \varepsilon p_1 + \dots) \end{aligned}$$

The aim is to take into account all the physical phenomena, it is thus necessary to include the parameter ε in the definition of some dimensionless numbers (table I) :

$$\begin{aligned} D &= \varepsilon^3 \tilde{D} & E &= \varepsilon \tilde{E} & M &= \varepsilon^{-1} \tilde{M} & S &= \varepsilon^{-3} \tilde{S} \\ H_j &= \tilde{H}_j & H_r &= \tilde{H}_r & H_c &= \tilde{H}_c & \phi &= \varepsilon \tilde{\phi} \\ CS &= \tilde{C}S & P &= \tilde{P} & C &= \tilde{C} \end{aligned}$$

where the tilded quantities are of order 1, and in the following, we will omit tildes.

If we substitute these definitions in the system of dimensionless equations, at first order, we obtain an equation to describe the evolution of the film thickness (details will be published elsewhere). If we go back to the initial coordinates (x, y, z, t) , we obtain a fourth order differential equation:

$$\begin{aligned} \partial_t \xi + E\mathcal{J} + \nabla \cdot \left[\frac{\xi^3}{3} \frac{dp_d}{d\xi} \nabla \xi \right] + \nabla \cdot [S\xi^3 \nabla (\Delta \xi)] \\ - \nabla \cdot [MP^{-1} \xi^2 \nabla (C_1 \xi)] - \nabla \cdot [D^{-1} E^2 \mathcal{J} \xi^3 \nabla \mathcal{J}] = 0 \end{aligned} \quad (30)$$

where the mass flux $\mathcal{J} = \lambda C_2 - C_1$. The effects of the disjoining pressure and of the curvature on the saturation temperature as well as the thermal conductivity of the vapour and at the substrate are included in variables C_1 and C_2 :

$$C_1 = \frac{N_1}{D} \quad C_2 = \frac{N_2}{D}$$

where

$$\begin{aligned} N_1 &= (\xi - H_r \lambda - \chi)(\phi \Omega - 1) + (1 + H_c) H_j \lambda (H_c(\phi \Omega - 1) - 1) \\ N_2 &= \phi \Omega (CS + H_c H_j + \xi - (1 + H_c) H_j) \\ D &= CS((1 + H_c)^2 H_j \lambda - H_r \lambda - \chi) + H_j (H_r \lambda + \chi) \\ &\quad + (CS - H_r \lambda + H_j((1 + H_c)^2 \lambda - 1) - \chi) \xi + \xi^2 \end{aligned}$$

with $\Omega = (p_d - p_\sigma)$ and χ the height at which the vapour temperature is equal to the saturation temperature.

The relation (30) is composed of various terms: the first one represents the temporal evolution of the thickness, the second one the mass loss, the third one the disjoining pressure, the fourth one the surface tension, the fifth one the thermocapillarity and the sixth one the vapour recoil.

III. STABILITY ANALYSIS

In order to study the linear stability of thin film, we write its thickness as the superposition of a flat reference state and small normal mode disturbances

$$\xi = \xi_0^*(t) + \varepsilon \sum_k \overline{\xi_k(0)} \exp^{\sigma_k t} \exp^{ikx} \quad (31)$$

where $\xi_0^*(t)$ is the state of reference i.e. a particular solution of Eq.(30), ε a small parameter, k is the wavenumber, $\overline{\xi_k(0)}$ is the initial amplitude and σ_k the growth rate of the mode of wavenumber k .

Eq.(30) being very complex, the stability is carried out by neglecting the repulsive Van der Waals forces ($R = 0$), the thermal resistance of the solid ($CS = 0$), the thermal conductivity of the vapour ($\lambda = 0$) and the jump of temperature across the interface ($L_{qq} \rightarrow \infty$). In this case, the phenomenological law (29) is reduced to

$$T_l = -H_j \mathcal{J} + \phi(p_d - p_\sigma)$$

If we pose $\phi = 0$, this equation is similar to the Hertz-Knudsen relation, that is obtained from the kinetic theory as used e.g. by Burelbach et al. [2]. The coefficient H_j is then given by

$$H_j = -\frac{(2-f)(\rho_l - \rho_v)\lambda_l T_{sat}}{2f\xi_0 \mathcal{L}^2 \rho_l \rho_v} \sqrt{\frac{2\pi R_g T_{sat}}{M_w}}$$

where R_g is the gas constant, M_w is the molecular weight and f is the evaporation coefficient. With these hypotheses, the evolution equation for the thickness reduces to

$$\begin{aligned} \partial_t \xi - \nabla \cdot \left[\frac{A \nabla \xi}{\xi} - S \xi^3 \nabla (\Delta \xi) + MP^{-1} \xi^2 \nabla (C_1 \xi) \right] \\ + D^{-1} E^2 \mathcal{J} \xi^3 \nabla \mathcal{J} + E\mathcal{J} = 0 \end{aligned} \quad (32)$$

with $\mathcal{J} = -C_1 = \frac{-A\phi + \xi^3(x,t)(1-3S\phi\Delta\xi(x,t))}{\xi^3(x,t)(\xi(x,t)-H_j)}$.

To analyse the stability of the film, we substitute (31) in (32) and carry out the development of the result in series of power of ε . We can then study the various orders. In this work, because of evaporation, we must take into account at least two orders: order 0 and order ε^1 .

A. At leading order (i.e. $\varepsilon \rightarrow 0$)

At the lowest order, we have

$$\partial_t \xi_0(t) = -\frac{E [\xi_0^3(t) - A\phi]}{\xi_0^3(t)(\xi_0(t) - H_j)} \quad (33)$$

As the Hamaker constant is positive ($A > 0$), this equation admits a stationary solution ($\xi_0 = \sqrt[3]{A\phi}$), which results from the equilibrium between the evaporation and the attractive intermolecular interactions. Fig. 2 illustrates 3 solutions of Eq.(33). We can observe that the thickness always converges towards $\sqrt[3]{A\phi}$, proving that the stationary film is stable to homogeneous disturbance.

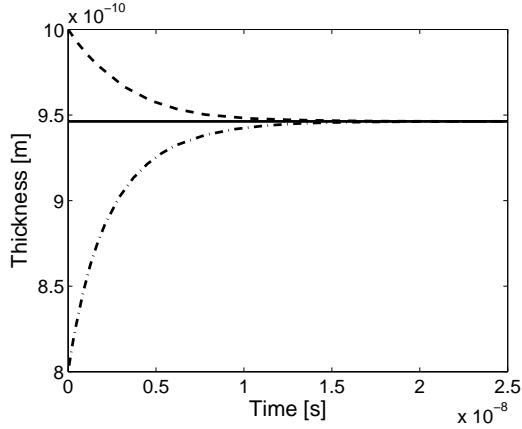


Fig. 2. Solutions of Eq.(33) for various initial conditions: $\xi(x, t = 0) = \sqrt[3]{A\phi} = 9.46$ Angström (solid line), $\xi(x, t = 0) > \sqrt[3]{A\phi}$ (dotted line) and $\xi(x, t = 0) < \sqrt[3]{A\phi}$ (dot-dashed line). The liquid used is ammonia (table II).

B. At first order

If we develop Eq.(32) at the next order in ϵ , we obtain the growth rate of the perturbations:

$$\sigma = \frac{(1 + \xi_0 k^2 S\phi) [\xi_0^3 k^2 (H_j + 3\mathcal{M}\phi - \xi_0) - 3E\phi]}{\xi_0(\xi_0 - H_j)\phi} \quad (34)$$

with $\xi_0 = \sqrt[3]{A\phi}$ and $\mathcal{M} = MP^{-1}$.

The stationary film will be stable if $\sigma < 0$ for all k . An analysis of Eq.(34) shows that this holds if

$$\mathcal{M} < \mathcal{M}_c = \frac{\xi_0 - H_j}{3\phi} \quad (35)$$

When $\mathcal{M} > \mathcal{M}_c$, a short-scale instability occurs, due to the variations of the local saturation temperature (Eq.(15)) inducing Marangoni convection.

IV. NUMERICAL TREATMENT

Eq.(30) is a strongly nonlinear partial differential equation. We will now look for its stationary solutions. The fourth order differential equation can be recast into a system of four ordinary differential equations. To solve this system, we used the software AUTO97 [11]. Integration requires initial conditions and boundary conditions. As initial conditions, we start with a flat film $\xi = \sqrt[3]{A\phi}$, i.e. all its derivatives set to zero. As boundary conditions, we impose in $x = 0$ the thickness of the film ($\xi = \sqrt[3]{A\phi}$), its first derivative ($\partial_x \xi = 0$), a small value for its second derivative ($\approx 10^{-7}$). Finally, we impose the curvature of the film (K_{end}) at the end of the integration domain ($x = L$). The value of $\partial_{x^3}^3 \xi$ adapts itself according to the final curvature.

$$\xi = \sqrt[3]{A\phi}; \quad \partial_x \xi|_{x=0} = 0; \quad \partial_{x^2}^2 \xi|_{x=0} = 10^{-7}; \quad \partial_{x^3}^3 \xi|_{x=L} = K_{end}$$

The advantage of being able to impose K_{end} , is to create a connection between the microscopic model and a macroscopic region, in order to simulate the entirety of a contact region. Indeed, the latter consists of three zones: an adsorbed film (where $\mathcal{J} = 0$), a microscopic region (model

described here) and a macroscopic part where the capillary pressure dominates. Consequently, the link between the two scales is established when: $K_{end} = K_{macro}$.

TABLE II
DATA FOR THE COMPUTATION OF THE PRESENTED
EXAMPLES (LIQUID: NH_3 AT $T_{sat} = 300K$).

Density of liquid (ρ_l): 600.0 kg m^{-3}
Density of vapour (ρ_v): 9.0 kg m^{-3}
Dynamic viscosity of liquid (ν_l): $2.16 \cdot 10^{-6} \text{ m}^2 \text{ s}^{-1}$
Evaporation coefficient (f): 1
Gas constant (R_g): $8.31 \text{ J K}^{-1} \text{ mol}^{-1}$
Hamaker constant (A): $2 \cdot 10^{-21} \text{ J}$
Molecular weight (M_w): $0.017 \text{ kg mol}^{-1}$
Specific heat of evaporation (\mathcal{L}): $118 \cdot 10^4 \text{ J kg}^{-1}$
Surface tension (γ): 0.02 N m^{-1}
Variation of surface tension with temperature (γ_r^s): $0.00005 \text{ N m}^{-1} \text{ K}^{-1}$
Thermal conductivity of liquid (λ_l): $0.480 \text{ W m}^{-1} \text{ K}^{-1}$

A. Validation of the model

In order to validate our model, we compared our solutions of Eq.(30) with those of Stephan and Busse [1]. Figs 3 and 4 illustrate the solutions for

$$MP^{-1} = 0 \quad D^{-1}E^2 = 0 \quad CS = 0 \quad R = 0$$

The fluid is ammonia at 300 K ; its properties are represented in table II. For this case, we choose $\xi_0 = 10^{-8} \text{ m}$ and the boundary conditions in Ref. [1] are $K_{macro} = 1.1 \text{ mm}^{-1}$ and $T_H = 301 \text{ K}$.

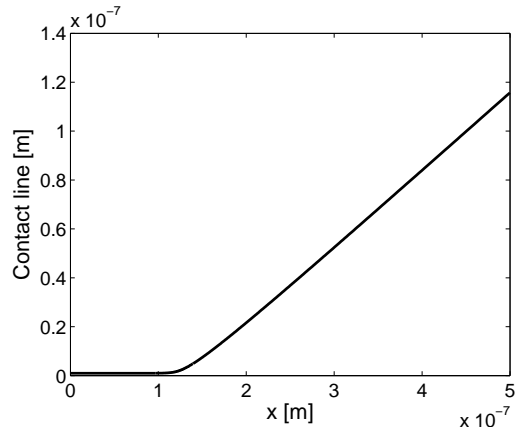


Fig. 3. Profile of the contact line shape

In the profile of the contact line (see Fig. 3), we can distinguish 3 zones. First, a film where the thickness (which is equal to 9.46 Angström) is such that the adhesion forces counterbalance evaporation (the heat flux is zero, see Fig. 4). Secondly, the microscopic zone. As soon as the thickness increases, the local saturation temperature decreases, which causes a variation of the heat flux: it increases strongly, reaches a maximum (5310 W cm^{-2} , Stephan and Busse found 5300 W cm^{-2}) and then drops.

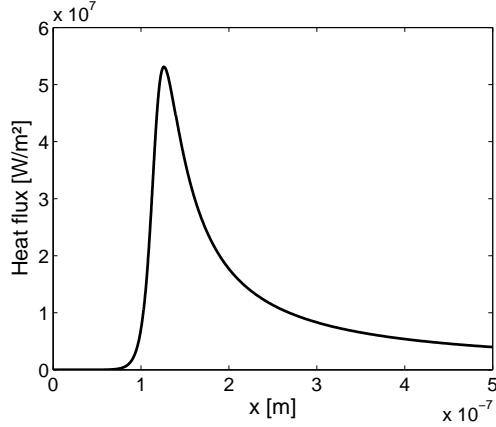


Fig. 4. Profile of the heat flux

At the maximum, the curvature is $9.89 \cdot 10^6 m^{-1}$ (the value of Stephan and Busse is $\approx 10^7 m^{-1}$). Thirdly: the macroscopic zone: the role of the disjoining pressure becomes negligible and the curvature of the contact line reaches the specified value and remains constant.

The total heat transferred in the micro region is

$$Q_{micro} = \int_{\xi_1}^{\xi_2} J_q d\xi = 3.23 W m^{-1}$$

with $\xi_1 = 0 m$ and $\xi_2 = 2 \cdot 10^{-7} m$ (for the same conditions, Stephan and Busse obtain $3.4 W m^{-1}$). Because of the slow decay of the heat flux ($J \propto \frac{1}{x}$ for $x \rightarrow \infty$), we cannot neglect the heat flux in the macro-region. So, to describe the evaporation near of a contact line, we must combine this model for the micro-region with the heat conduction equation in the macroscopic region.

B. Results and discussion

The model presented here is composed of many parameters which depend on the physical properties of the fluid and on external constraints. The figures below illustrate the behaviour of the heat flux and of the contact angle when some of these numbers vary. The microscopic contact angle is defined as the angle between the tangent at the interface and the wall. Our analysis concerns the following physical effects: firstly thermal resistance of the solid, secondly the overheating, thirdly the Marangoni convection, fourthly the variation of the local saturation temperature at the interface and fifthly the chemical potential non-equilibrium at the evaporating interface (parameter H_j). The numerical computations were carried out under the following conditions: the fluid is ammonia, $T_{sat} = 300 K$, $T_H = 301 K$ (when ΔT is not fixed) and $K_{macro} = 1.1 mm^{-1}$.

Figs 5 and 6 display the impact of the thermal resistance of the solid though the parameter CS on the microscopic contact angle and on the heat flux when $\mathcal{M} = 0$, $E^2 D^{-1} = 0$ and $R = 0$. If we assume that d_w , λ_l and ξ_0 are constant, we observe that when λ_s increases (i.e. when the thermal resistance of the solid decreases), the heat flux and the contact angle increase.

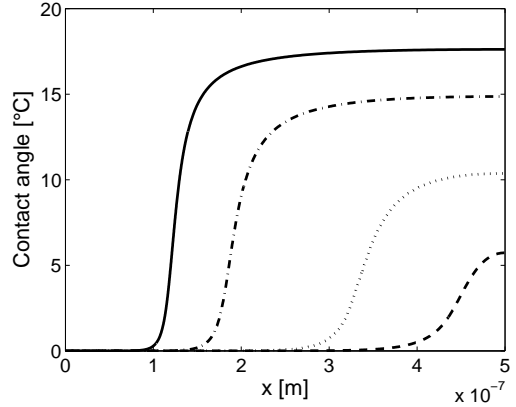


Fig. 5. The variation of the microscopic contact angle with the thermal resistance of the solid: $CS = 0$ (solid line), $CS = 1$ (dotted line), $CS = 5$ (dot-dashed line) and $CS = 10$ (dashed line).

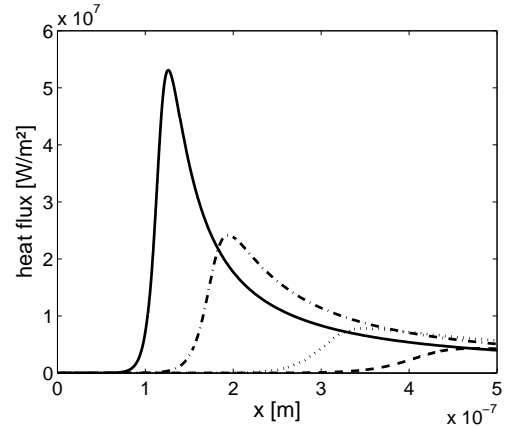


Fig. 6. The variation of the heat flux with the thermal resistance of the solid. Same legend as for Fig. 5

Figs 7 and 8 show the contact angle and the heat flux for various values of ΔT when $\mathcal{M} = 0$, $E^2 D^{-1} = 0$, $R = 0$ and $CS = 0$. We note that the heat flux and the contact angle increase with ΔT .

The influence of the Marangoni number is represented in Figs 9 and 10. These simulations are realised for: $E^2 D^{-1} = 0$, $R = 0$ and $CS = 0$. We can observe that, when \mathcal{M} increases, the peak of the heat flux decreases while the macroscopic value of the contact angle increases. The value of \mathcal{M} is limited: $\mathcal{M}_{max} \approx 1.7$. Beyond, instabilities appear. We find the conclusions of the linear stability analysis. Indeed, for $\Delta T = 1 K$, the Eq.(35) gives: $\mathcal{M}_c = 1.78$. Actually, this threshold is never reached. For example, for ammonia (with $\Delta T = 1 K$): $\mathcal{M} = 0.00887$.

Figs 11 and 12 show how the heat flux and the contact angle are affected by variations of the local saturation temperature at the interface (thanks to a variation of the parameter ϕ). In the computations, we assume that $\mathcal{M} = 0$, $E^2 D^{-1} = 0$, $R = 0$ and $CS = 0$. When increasing ϕ , the

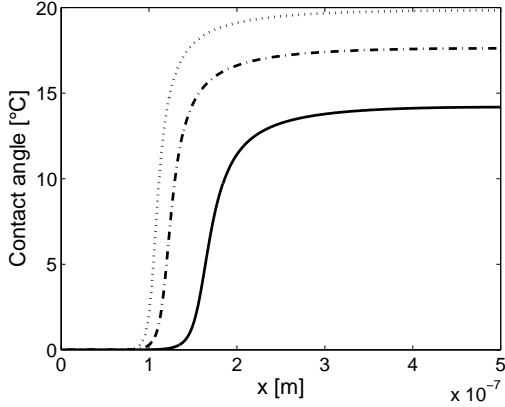


Fig. 7. The variation of the microscopic contact angle with ΔT : $\Delta T = 0.5 K$ (solid line), $\Delta T = 1 K$ (dot-dashed line) and $\Delta T = 1.5 K$ (dotted line).

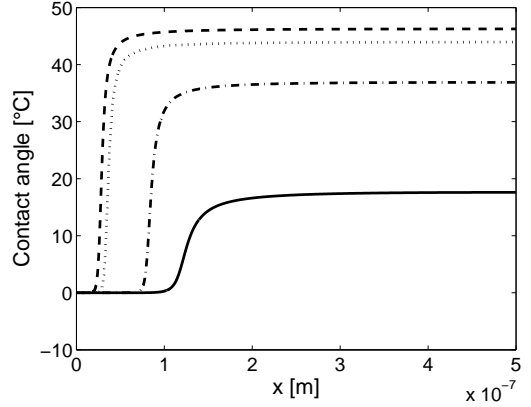


Fig. 9. The variation of the microscopic contact angle with Marangoni number: $\mathcal{M} = 0$ (solid line), $\mathcal{M} = 1$ (dot-dashed line), $\mathcal{M} = 1.5$ (dotted line) and $\mathcal{M} = 1.7$ (dashed line).

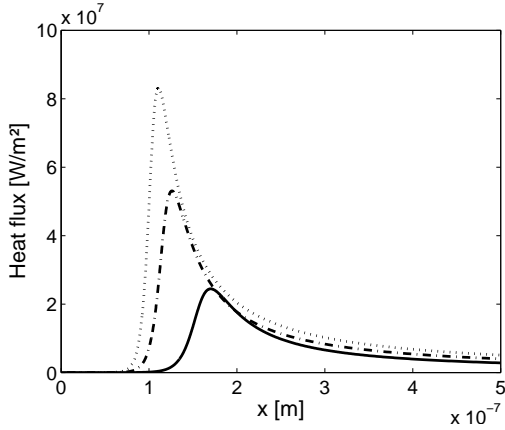


Fig. 8. The variation of the heat flux with ΔT . See Fig. 7 for legend.

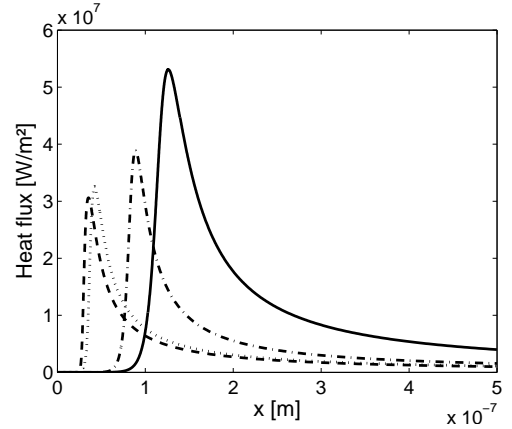


Fig. 10. The variation of the heat flux with Marangoni number. Same legend as for Fig. 9

effects of disjoining pressure and of the curvature on this temperature reduce the volatility of the liquid and cause a decrease of the heat flux and of the contact angle.

Figs 13 and 14 show how the non-equilibrium evaporation affects the heat flux and the contact angle in the case where $\mathcal{M} = 0$, $E^2 D^{-1} = 0$, $R = 0$ and $CS = 0$. As H_j increases (in absolute value), the kinetic resistance to evaporation increases and thus the heat flux drops. The contact angle decreases also.

V. CONCLUSIONS

Thanks to the lubrication theory, we developed a mathematical model for a thin liquid film in contact with a solid wall and its own vapour. We obtain an evolution equation for the film thickness when the interface is subject simultaneously to the following effects: surface tension, thermocapillarity, evaporation, vapour recoil, disjoining pressure, the temperature discontinuity between vapour and liquid and the variation of the saturation temperature. This equation generalized the result obtained by Burelbach et al. [2].

Neglecting the repulsive molecular forces, the thermal

conductivity of the vapour, the thermal resistance of the solid and the jump of temperature across the interface, we analyse the linear stability of this film. We showed that because of the influence of the disjoining pressure on $T_{sat,loc}$, an adsorbed film is possible (equilibrium between the evaporation and the attractive intermolecular interactions). This adsorbed film is stable, despite the destabilizing Marangoni effects, provided the Marangoni number is less than a critical value ($\mathcal{M} < \frac{\xi_0 - H_j}{3\phi}$).

Then, under particular conditions (generally we neglected the recoil pressure, the thermal conductivity of the vapour and the repulsive forces), we carried out numerical simulations in order to highlight the influence of different mechanisms on the heat flux and on the apparent contact angle. The former is supported by a great jump of temperature between the wall and the saturation temperature of the liquid (ΔT). On the other hand, it decreases when the thermal resistance of the solid, the Marangoni number, the variability of the local saturation temperature and the kinetic resistance to evaporation increase. Concerning the contact angle, we can conclude that it increases with ΔT

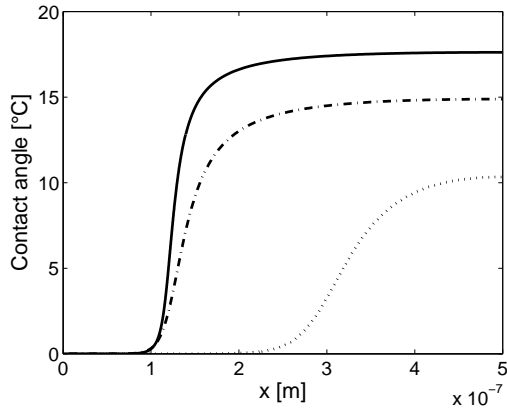


Fig. 11. The variation of the microscopic contact angle with ϕ : $\phi = 0.11935$ (solid line), $\phi = 1$ (dot-dashed line) and $\phi = 5$ (dotted line).

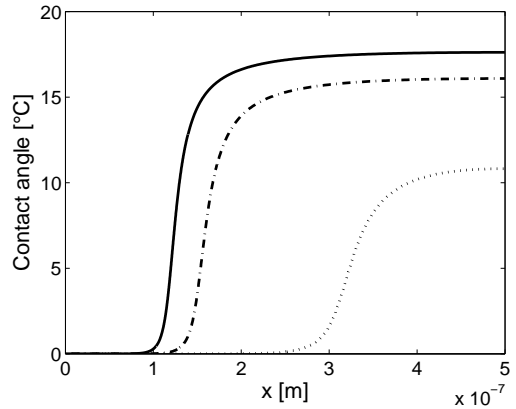


Fig. 13. The variation of the microscopic contact angle with H_j : $H_j = -0.5429$ (solid line), $H_j = -1$ (dot-dashed line) and $H_j = -5$ (dotted line).

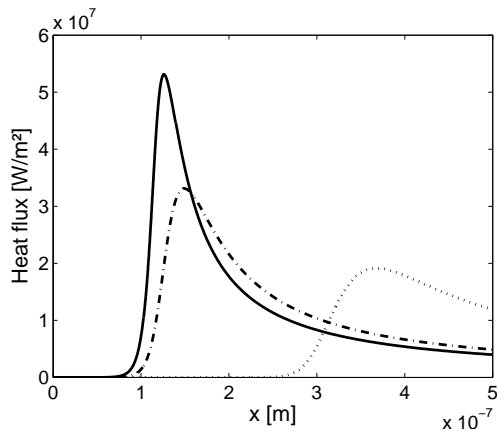


Fig. 12. The variation of the heat flux with ϕ . See Fig. 11 for legend.

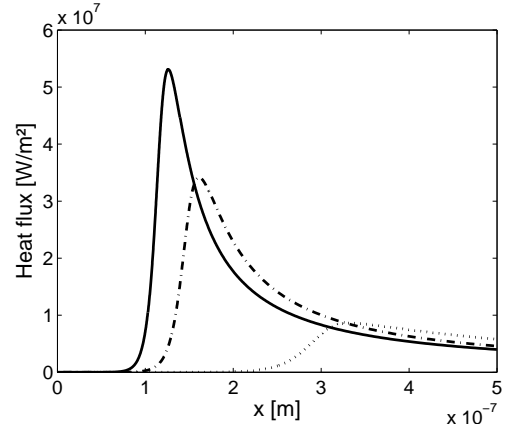


Fig. 14. The variation of the heat flux with H_j . Same legend as for Fig. 13

and the Marangoni number while it decreases when the thermal resistance of the solid, the variability of the local saturation temperature and the kinetic resistance to evaporation increase.

ACKNOWLEDGMENTS

The authors acknowledge interesting discussions with P.Stephan, L.Tadrist and N.Nilolayev. SR and PC respectively acknowledge financial support of the FRIA (Fonds pour la Formation la Recherche dans l'Industrie et l'Agriculture) and FNRS (Fonds National de la Recherche Scientifique). This work was partially financed by the CIMEX and BOILING projects funded by the European Space Agency, and the ARCHIMEDES project funded by the "Communauté française de Belgique - Actions de Recherche Concertées".

REFERENCES

- [1] P.C. Stephan and C.A. Busse, *Analysis of the heat transfer coefficient of grooved heat pipe evaporator walls*. Int. J. Heat Mass Transfer, 35(2), 383-391, 1992.
- [2] J.P. Burelbach, S.G. Bankoff, and S.H. Davis, *Nonlinear stability of evaporating/condensing liquid films*. J. Fluid Mech., 195: 463-494, 1988.

- [3] D. Bedeaux, L.J.F. Hermans and T. Ytrehus, *Slow Evaporation and Condensation*. Physica A, 169, 263-280, 1990.
- [4] G. Fang and C.A. Ward, *Phys. Rev E* 59, 417, 1999.
- [5] Alexander Oron, Stephen H. Davis and S.George Bankoff, *Long-scale evolution of thin liquid films*. Reviews of Modern Physics, 69(3): 931-980, 1997.
- [6] Vladimir S. Ajaev, *Viscous flow of a volatile liquid on an inclined heated surface*. J. Colloid Interface Sci., 280, 165-173, 2004.
- [7] P. Colinet, J.C. Legros and M.G. Velarde, *Nonlinear Dynamics of Surface-Tension-Driven Instabilities*. Wiley-VCH, Berlin, 2001.
- [8] B.V. Derjaguin, N.V. Churaev and V.M. Muller, *Surface Forces*. Consultants Bureau, New York, 1987.
- [9] V.P.Carey, *DSMC modeling of near-interface transport in liquid-vapor phase-change processes with multiple microscale effects, Developments in Heat Transfer (volume 13, chapitre 8) - Heat and Fluid Flow in Microscale and Nanoscale Structure*. Eds M. Faghri and B. Sunden, Witpress, Boston, 2004.
- [10] J. Margerit, P. Colinet, G. Lebon, C.S. Iorio and J.C. Legros, *Interfacial nonequilibrium and Bénard-Marangoni instability of a liquid-vapor system*. Phys. Rev E, 68, 041601-1 041601-14, 2003.
- [11] E.J. Doedel, A.R. Champneys, T.F. Frairfieve, Y.A. Kuznetsov, B. Sandstede, and X. Wang, *Auto97: Continuation and bifurcation software for ordinary differential equations*. Montreal Concordia University, 1997. AUTO97 and its HOMCONT package are freely distributed and can be found on the web for example at the address: <ftp.concordia.ca/pub/doedel/auto>.